

# Critical behaviors in central and peripheral collisions: a comparative analysis

M. D'Agostino<sup>(1)</sup>, M. Bruno<sup>(1)</sup>, F. Gulminelli<sup>(2)</sup>, R. Bougault<sup>(2)</sup>,  
F. Cannata<sup>(1)</sup>, Ph. Chomaz<sup>(3)</sup>, F. Gramegna<sup>(4)</sup>, N. Le Neindre<sup>(3,1)</sup>,  
G. V. Margagliotti<sup>(5)</sup>, A. Moroni<sup>(6)</sup>, G. Vannini<sup>(1)</sup>, J. P . Wieleczko<sup>(3)</sup>

(1) *Dipartimento di Fisica and INFN, Bologna, Italy*

(2) *LPC Caen (IN2P3-CNRS/ISMRA et Université),  
F-14050 Caen Cédex, France*

(3) *GANIL (DSM-CEA/IN2P3-CNRS),  
B.P.5027,F-14021 Caen Cédex, France*

(4) *INFN Laboratorio Nazionale di Legnaro, Italy*

(5) *Dipartimento di Fisica and INFN, Trieste, Italy*

(6) *Dipartimento di Fisica and INFN, Milano, Italy*

Quasi-projectile events from peripheral 35 *A.MeV Au+Au* collisions are compared to central *Au + C*, *Au + Cu* and *Au + Au* events in the same range of excitation energy in terms of critical partitions and critical exponents. All the different data sets coherently point to a value  $E_c^* = 4.5 \text{ A.MeV}$  for the apparent critical excitation energy. The critical exponents  $\tau, \sigma$  are compatible with the observation of a liquid-gas phase transition for these systems.

PACS numbers: 24.10.Pa,64.60.Fr,68.35.Rh

## I. INTRODUCTION

Multifragmentation has been tentatively connected to a critical phenomenon [1] since the first heavy ion experiments. The recent determination of a consistent set of critical exponents in different multifragmentation data [2, 3] tends to confirm this hypothesis though finite size corrections to scaling are unknown to a large extent.

Deviations from critical behavior have been however observed for heavy sources [4, 5,

6, 7, 8] formed in central collisions and the question arises whether the multifragmentation mechanism depends on the entrance channel. Indeed thermal scaling near a critical point is expected in the case of equilibrated sources, which decay independently of the way they were formed. High energy experiments [4, 5] observe partitions strongly governed by the collective energy, and the deviations of the charge distribution from a power law of exponent  $\tau \approx 2$  can be explained by dynamical models [9].

However, an apparent exponent  $\tau \ll 2$  has been observed [6, 7, 8] also in central collisions measured at intermediate incident energies where collective components, if any, represent a small correction to the thermal excitation energy. A tentative explanation of this phenomenon suggests that Coulomb interaction would prevent heavy charged systems to attain statistical equilibration [10].

In the following, by comparing Quasi-Projectile events from peripheral 35 *A.MeV Au+Au* collisions and central collisions of the asymmetric *Au + Cu* reactions at 25 and 35 *A.MeV* incident energy, we will show that in the latter case the increase of the Coulomb strength with respect to a *Au* source leads to asymptotic partitions of early emitted fragments coexisting with secondary decay products. Once this sequential emission is backtraced, thermal scaling is observed for several moments of charge distributions in good agreement with the QP data.

A multiparametric fit within a Fisher droplet ansatz [11, 12] allows to analyze two additional data samples (central *Au + C* and *Au + Au*), at excitation energies far away from the expected critical energy.

Within this ansatz all the reactions consistently point to the same set of critical exponents and give indication that the critical excitation energy is  $E_c^* = 4.5 \pm 0.5 \text{ A.MeV}$ . Only for the heaviest system (central *Au + Au* at 35 *A.MeV*) a deviation from thermal scaling is observed, but more data at lower incident energy are needed to confirm this point.

The plan of the paper is as follows. After a short presentation in Section II of the different data samples collected at the NSCL National Laboratory with the MULTICS-MINIBALL apparatus, the scaling properties of *Au* Quasi-Projectiles detected in peripheral collisions of the 35 *A.MeV Au+Au* reaction will be reviewed in Section III. The different central data sets are presented in Section IV, where the correlation function technique to backtrace secondary fission is explained, and analyzed in Section V in terms of Fisher scaling. Conclusions are drawn in Section VI.

## II. EXPERIMENT

All the measurements discussed in this paper were performed at the K1200-NSCL Cyclotron of the Michigan State University. The MULTICS and MINIBALL arrays were coupled to measure charged products, with a geometric acceptance larger than 87% of  $4\pi$ . More experimental details have been reported in Ref. [13].

Peripheral collisions of predominantly binary character were selected for the reaction  $Au + Au$  at 35 A.MeV [3]. A Quasi-Projectile source of nearly constant charge and excitation energy from 1 to about 8 A.MeV was reconstructed through an event shape analysis. The fragment angular distributions [14] are compatible with an isotropic emission. The reproduction of the experimental charge partitions by statistical model calculations [16] is consistent with a good degree of source equilibration [3, 15].

For the reactions  $Au + Cu$  at 25 and 35 A.MeV the most central 10% of the total measured cross section was selected by a charged particle multiplicity cut. Well detected events (total detected charge larger than 90% of the total charge) were analyzed in terms of event shape and the selected almost spherical events ( $\Theta_{flow} \geq 60^\circ$ ) are hereafter presented. The same procedure has been followed to select central events in the  $Au + Au$  reaction, while in the  $Au + C$  collision at 25 A.MeV the average fragment multiplicity  $\langle M \rangle = 2.2$  (standard deviation 0.2) is too low to perform any shape analysis and only the total multiplicity and total detected charge cut have been applied.

Mass numbers for clusters of charge 1 and 2 were measured. To determine the cluster mass distribution, clusters of a given charge  $Z$  were counted on an event by event basis and it was assumed that  $N(A) = N(Z)$ . Checks were made on the influence of the mass estimation. Our main conclusions do not change if we estimate the cluster mass from the  $A_0$ -to- $Z_0$  ratio of the fragmenting system or we assume the mass of stable nuclei.

## III. QP SOURCE : SCALING OF STATIC OBSERVABLES

Renormalization group (RG) arguments lead, near the critical point, size distributions scaling as [17]

$$n(A, \epsilon) = qA^{-\tau} f(\epsilon A^\sigma) \quad (1)$$

where  $n(A) = N(A)/A_0$  is the cluster distribution normalized to the size of the fragmenting system,  $\epsilon$  measures the distance from the critical point ( $\epsilon = (E_c^* - E^*)/E_c^*$  for events sorted in excitation energy bins),  $q$  is a normalization constant [17, 18],  $f$  is the scaling function and  $\tau, \sigma$  are universal critical exponents.

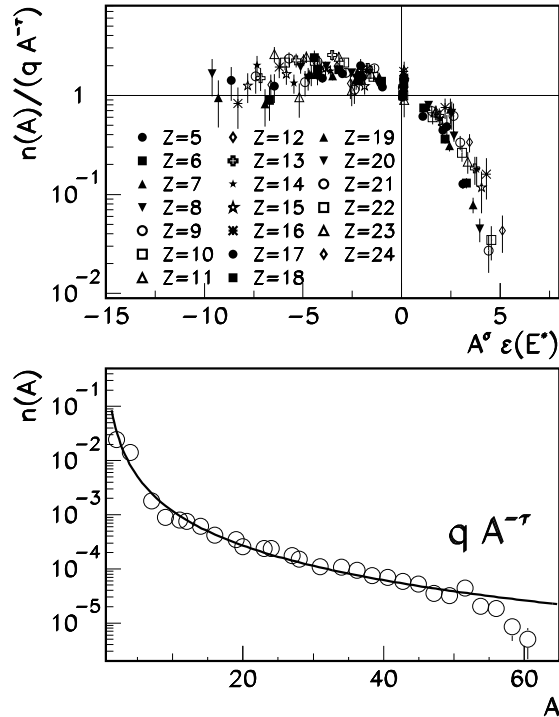


FIG. 1: *Peripheral Au + Au collisions. Top panel: scaling function for the QP source with the ansatz eq.(1). Bottom panel: mass distribution of the QP decay products in the range  $4 \leq E^* \leq 5$  A.MeV, line: power law with  $\tau = 2.12$  [3].*

For peripheral  $Au + Au$  collisions the critical exponents as well as the critical excitation energy of the Quasi-Projectile source (QP) were extracted from the analysis of the moments of the charge distribution [3]. The critical exponents ( $\tau = 2.12, \sigma = 0.64$ ) form a consistent set and are close to the values of the liquid-gas universality class. Near the excitation energy identified as critical from the behavior of the biggest fragment [3],  $E_c^* \approx 4.5$  A.MeV, the size distribution is well described by a power law of exponent  $\tau = 2.12$  as shown in the bottom panel of Fig.1.

By applying eq.(1) to the QP events, a scaling behavior is observed (Fig.1 top panel) over the whole range in excitation energy (from 1 to about 8 A.MeV) and fragment charge

$5 \leq Z \leq 24$ . Since for the lightest fragments side feeding or non-equilibrium effects could affect the final production rate, fragments with  $Z < 5$  were discarded.

In recent papers [12, 18] Elliott et al. analyze the critical behavior of the size distribution in terms of the Fisher droplet model. In this model [11] the vapor coexisting with a liquid in the mixed phase of a liquid-gas phase transition is approximated by an ideal gas of clusters. A scaling around the critical point, similar to eq.(1) is assumed, but a different form is suggested for the scaling function

$$n(A, T) = qA^{-\tau} \exp\left(\frac{\Delta G(A, T)}{T}\right) \quad (2)$$

where  $\Delta G(A, T)$  represents the variation of the Gibbs free energy upon formation of a drop of  $A$  nucleons out of an homogeneous nuclear vapor at temperature  $T$

$$\Delta G(A, T) = A\Delta\mu - c_0\epsilon A^\sigma \quad (3)$$

Here  $\Delta\mu$  represents the difference in chemical potential between the two phases,  $\epsilon$  measures the distance from the critical point  $\epsilon = (T_c - T)/T_c$ , and  $c_0$  is the surface energy coefficient. This expression can be extended to charged systems [19] by calculating [16] the Coulomb part of the free energy  $\delta C$  in the Wigner-Seitz approximation

$$\Delta G_{tot}(A, Z, T) = \Delta G(A, T) - \delta C = \Delta G(A, T) - \frac{3}{5}e^2 \frac{Z^2}{R} \left(1 - (1 - c_c \epsilon^\beta)^{1/3}\right) \quad (4)$$

where  $R$  is the radius of a fragment of mass  $A$ ,  $c_c$  is a constant related to the density of the liquid phase [19] and  $\beta$  is a critical exponent.

To verify the ability of this ansatz to extract information about criticality, we performed a multi-parameter fit of the QP data (over 200 data points). The values of the critical parameters from the fit were then compared with those already known from the analysis of the moments of the charge distribution [3].

As in Ref. [12] the temperature  $T$  in eqs.(2, 3) has been replaced by  $\sqrt{8E^*/A}$ . This ansatz has not to be interpreted as a realistic temperature estimator, since the assumption that close to the critical point nuclear systems behave like a degenerate Fermi gas is highly disputable and not supported by experimental data [20]. This Fermi gas ansatz has only to be considered as an effective parameterization of the scaling function which allows a direct and quantitative comparison with the similar analysis performed on Isis data [12].

In principle  $\Delta\mu$  as well as  $c_0$  [12] and  $c_c$  can depend on temperature. To keep parameters under control we have taken the simplest parameterizations that allows a good quality fit of the whole cluster size distribution.  $c_0$  and  $c_c$  were treated as free parameters, independent from the temperature, the exponent  $\beta$  was fixed at the value  $1/3$  as resulted from previous analysis on the QP source [3]. Whatever is the parameterization chosen for  $\Delta\mu$ , its value at  $E^* = E_c^*$  is compatible with zero.

<b>Peripheral collisions</b>	$\tau$	$\sigma$	$E_c^*$ (A.MeV)	$c_0$	$\chi^2$
$\delta C = 0, \Delta\mu$ fixed at 0	$2.05 \pm 0.01$	$0.66 \pm 0.06$	$4.19 \pm 0.06$	$3.3 \pm 0.6$	1.5
$\delta C = 0, \Delta\mu = const.$	$2.07 \pm 0.02$	$0.70 \pm 0.03$	$4.5 \pm 0.4$	$3.0 \pm 0.3$	1.6
$\delta C = 0, \Delta\mu = f(T)$	$2.10 \pm 0.02$	$0.66 \pm 0.02$	$4.5 \pm 0.1$	$8.0 \pm 0.3$	1.3
$\delta C$ eq.(4), $\Delta\mu = f(T)$	$2.08 \pm 0.02$	$0.66 \pm 0.02$	$4.40 \pm 0.05$	$10.9 \pm 0.4$	1.7

TABLE I: Values of the critical exponents  $\tau$ ,  $\sigma$ , critical excitation energy  $E_c^*$ , surface energy coefficient  $c_0$  and  $\chi^2$  of the Fisher scaling fit through Eq.s(2,3,4).

In Table I we report the results obtained for two different parameterizations for  $\Delta\mu$  (a constant value or a polynomial of order two in  $E^*/A$ ) together with some results obtained switching on/off the Coulomb term of eq.4. Checks were also made on the parameterization chosen for the Coulomb term. Results compatible with those reported in Table I are obtained with the parameterization used in Ref. [12].

The fit through Fisher scaling function (eq.2 and following) produces a scaling behavior for the data, comparable to the RG ansatz as can be seen in Fig.2 (bottom panel). Critical exponents and the critical excitation energy, reported in Table I, are in agreement with the previous analyses [3] of the moments of the charge distribution. It is interesting to remark that similarly to the RG ansatz the scaling obtained with the Fisher scaling function is observed in the sub-critical and in the supercritical domain, even if in the context of the Fisher model eq.(2) has no physical meaning for  $E^* > E_c^*$ . This is more quantitatively shown in Figure 2 (top panel) which compares the measured production yields of a few clusters with the results of the fit. As already observed in Ref. [21] a parameterization  $\Delta\mu = f(T)$  allows the Fisher scaling function to reproduce the data well above the critical excitation energy. On the contrary, when  $\Delta\mu$  is treated as a constant, the scaling is observed, mainly for large cluster sizes, only up to the critical excitation energy.

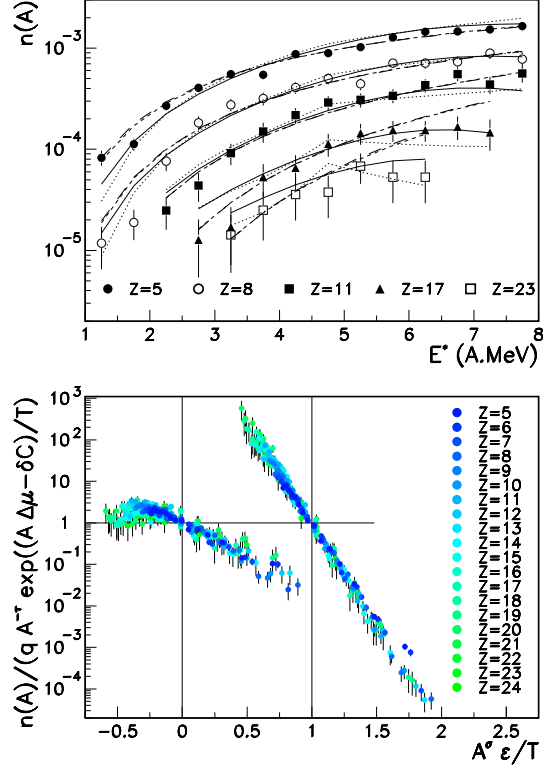


FIG. 2: *Top panel: Cluster yields of the QP source as a function of the excitation energy (symbols) and fits with eq.(2). Dotted line:  $\delta C$  eq.(4) and  $\Delta\mu = f(T)$ , solid line:  $\delta C = 0$  and  $\Delta\mu = f(T)$ , short dashed line:  $\delta C = 0$ ,  $\Delta\mu = 0$ , long dashed line:  $\delta C = 0$ ,  $\Delta\mu = \text{const.}$ . Bottom panel: scaled yield distribution versus the scaled temperature for the cases:  $\delta C = 0$ ,  $\Delta\mu = 0$  (left) and  $\Delta\mu = f(T)$  (right). To visualize the results on the same picture a constant horizontal shift  $C = 1$  is given to the latter distribution.*

The similarity of the results obtained with the RG and with the Fisher scaling demonstrates that the values of the critical parameters are very robust with respect to the detailed shape assumed for the scaling function. On the other hand this also implies that the adequacy of the Fisher ansatz to the data is not a sufficient condition to give any detailed physical meaning to the value of the fit parameters  $\Delta\mu$ ,  $c_0$ ,  $c_c$  nor to the sorting parameter  $\sqrt{8E^*/A}$ . As an example, the quality of the fit and the value of the critical parameters do not drastically change if one suppresses the Coulomb as well as the volume term [18] (see Table I); the value of  $c_0$  strongly depends on the parameterization of the scaling function and the full scale of the scaled yields depends also on the level density parameter assumed to estimate the temperature.

<b>Peripheral collisions</b>	$\tau$	$\sigma$	$E_c^*$ (A.MeV)	$c_0$	$\chi^2$
$E^* = 1 - 2$ (A.MeV)	$2.5 \pm 0.2$	$0.66 \pm 0.03$	$4.5 \pm 0.6$	$10.0 \pm 0.7$	1.4
$E^* = 2 - 3$ (A.MeV)	$2.1 \pm 0.1$	$0.65 \pm 0.03$	$4.5 \pm 0.3$	$10.0 \pm 0.9$	1.
$E^* = 3 - 4$ (A.MeV)	$2.10 \pm 0.08$	$0.68 \pm 0.05$	$4.5 \pm 0.2$	$10.0 \pm 1.5$	0.7
$E^* = 4 - 5$ (A.MeV)	$2.08 \pm 0.04$	$0.66 \pm 0.02$	$4.5 \pm 0.2$	$10. \pm 5.$	1.0
$E^* = 5 - 6$ (A.MeV)	$2.08 \pm 0.02$	$0.66 \pm 0.06$	$4.50 \pm 0.02$	$10.1 \pm 0.2$	1.1
$E^* = 6 - 7$ (A.MeV)	$2.08 \pm 0.02$	$0.66 \pm 0.04$	$4.50 \pm 0.02$	$10.1 \pm 0.1$	1.5
$E^* \geq 7$ (A.MeV)	$2.08 \pm 0.02$	$0.66 \pm 0.03$	$4.46 \pm 0.02$	$10.0 \pm 0.1$	1.1

TABLE II: Values of the critical exponents  $\tau$ ,  $\sigma$ , critical excitation energy  $E_c^*$ , surface energy coefficient  $c_0$  and  $\chi^2$  of the Fisher scaling fit through Eq.s(2,3,4) in bins of excitation energy.

The Fisher scaling procedure has also been performed on several intervals of the excitation energy and the results are summarized in Table II. This test allows to validate a Fisher scaling analysis on central collisions, where the excitation energy is distributed in a narrow interval.

As can be seen in Table II for all the energy intervals the fitting procedure recognizes the same critical point even if the critical energy is not contained in the set of data. The critical exponents are again in agreement with those previously obtained.

The uncertainty in the critical exponents and in the critical excitation energy decreases for increasing  $E^*$ , signaling that only an approximate description of the critical region can be provided by events containing information only on the vapor, as previously found in the study performed in Ref. [21] on Lattice Gas events. Another signal is given by the value of  $\Delta\mu$  at  $E_c^*$ . While this value is compatible with zero for all the excitation energy bins  $E^* > 2$  A.MeV, this is not the case for the first interval of excitation energy, where it results  $\Delta\mu(E^* = E_c^*) = 7.2 \pm 0.1$  A.MeV. This does not seem merely related to the distance from the critical excitation energy : indeed “overcritical” events 2 A.MeV above  $E_c^*$  recognize the critical point better than events 2 A.MeV below.

To conclude, we have shown that the Fisher scaling technique is extremely powerful for the determination of the critical exponents and the critical excitation energy. However, the adequacy of the Fisher ansatz to the data is not sufficient to give a physical meaning to the other fit parameters.



## IV. CENTRAL COLLISIONS

### A. Equilibration of the emitting sources

We have shown in the previous Section that a critical-like behavior is observed around  $E_c^* = 4.5 A.MeV$  for QP events. To explore the effect of the entrance channel and/or the size of the system we will now turn to the analysis of central collisions.

Firstly we show that the considered central events are compatible with the decay of equilibrated sources and therefore can be good candidates for an analysis in terms of thermal scaling. The relevance of the thermostatistical analysis depends indeed on the approximation at which an equilibrium is realized. As a general statement, the degree of approximation of an equilibrium is indicated by the degree of the agreement of data with statistical models containing the same constraints as the data.

To check the quality of the source selection criteria, a standard procedure consists in verifying that events are spherically symmetric in momentum space. Of course it is very

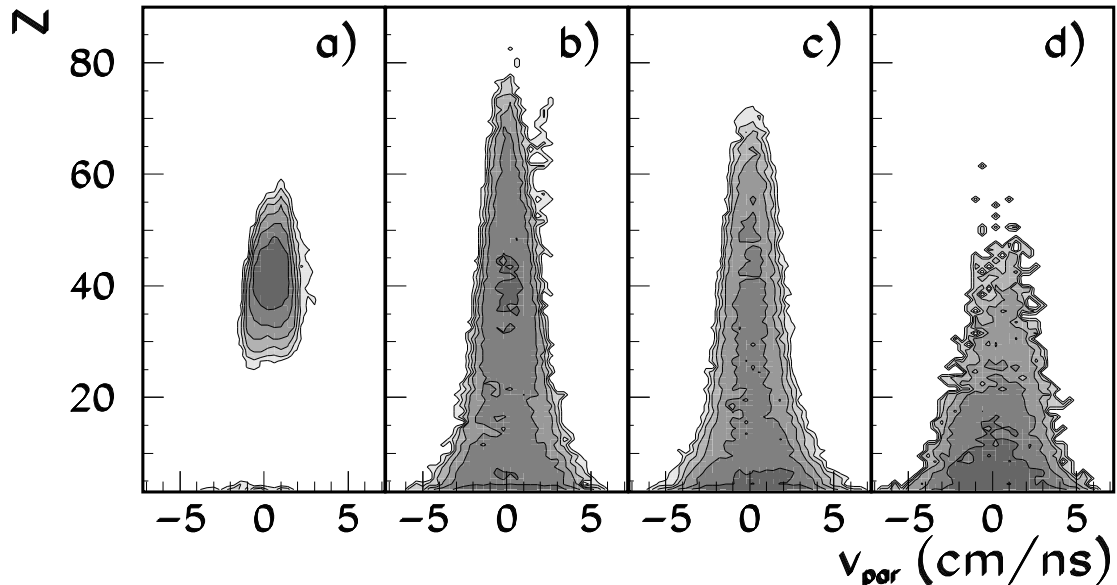


FIG. 3: *Fragment charge  $Z$  versus the parallel velocity along the beam direction in the center of mass reference frame for central  $Au + C$  events at 25 A.MeV (panel a),  $Au + Cu$  events at 25 (panel b) and 35 A.MeV (panel c) and  $Au + Au$  central collisions at 35 A.MeV (panel d).*

likely that in the dynamical preparation of the nuclear source the shape degree of freedom

may not be completely relaxed; such a case could in principle be addressed within a statistical ensemble where deformation is explicitly accounted for. However restricting the analysis to spherical systems guarantees that preequilibrium effects do not pollute the statistical sample.

An observable suggested [22] to discriminate between single source and multiple sources decay events, is the correlation between the velocity along the beam direction and the charge of the fragments.

This observable is shown in Fig.3 for central collisions of the reactions  $Au + C$  at 25 A.MeV incident energy (panel a),  $Au + Cu$  at 25 (b), 35 A.MeV (c) and  $Au + Au$  at 35 A.MeV (d). In this representation one can observe that the source is at rest in the centre of mass reference frame and also that the general trend for fragments is to be isotropically emitted.

In Figure 4 we compare the charge distributions to the predictions of statistical models.

The  $Au + C$  data are the standard prototype of low energy compound nucleus deexcitation. Due to the strongly forward focused kinematics and to the minimum detection angle ( $\theta_{lab} > 3^\circ$ ), complete events are detected only in the case of fission of the compound. The charge distribution displayed in Figure 4 (top panel) is well reproduced by the Gemini [23] code, which describes fragment production as a sequence of binary fission-like emissions. The excitation energy needed to the model to reproduce the experimental distribution (1.4 A.MeV) agrees with the experimental value. The small shift between the experimental and simulated charge distributions is presumably due to the (small) difference between the size of the experimental and simulated source. While Gemini can not be run for sources heavier than  $Au$ , in the data the charge collected by the two fission fragments is the charge of the completely fused system.

The charge distribution of the central collisions extracted from the  $Au + Cu$  25 and 35 A.MeV reaction are compared to statistical SMM model calculations [16], where the mass of the fragmenting source has been assumed equal to the total mass of the system and the freeze out volume has been taken as  $V = 3V_0$ . The model well reproduces the data with input excitation energies (3.3 and 4.1 A.MeV for the 25 and 35 A.MeV data respectively) close to the average energies measured by calorimetry.

In the case of the 35 A.MeV  $Au + Cu$  sample the excitation energy is close to the value where the QP shows critical partitions with  $\tau \simeq 2$ . However, as it appears from Fig.4, the central events distribution is much flatter and can be approximately fitted only with an

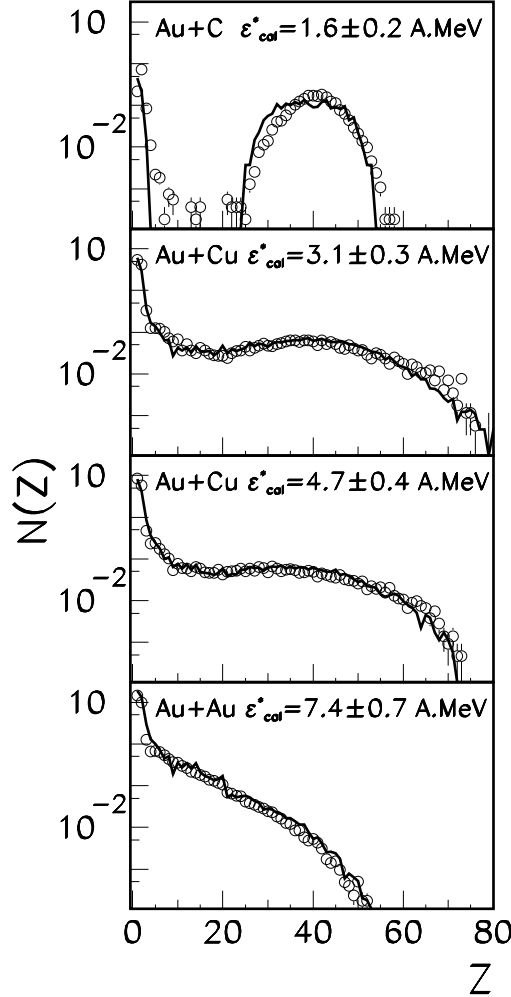


FIG. 4: Symbols: inclusive charge distributions for central  $Au+C$  events at 25  $A.MeV$ ,  $Au+Cu$  at 25, 35  $A.MeV$  and  $Au+Au$  at 35  $A.MeV$  from top to bottom, respectively. The reported excitation energy and standard deviation are the experimental calorimetric values for each sample. Lines: filtered GEMINI (top panel) and SMM (other panels) simulations.

effective exponent  $\tau_{eff} \simeq 1.4$ . The average excitation energy is lower for the 25  $A.MeV$   $Au+C$  sample, however also for this reaction a two parameter power law fit of the distribution gives an apparent exponent  $\tau_{eff} \simeq 1.4$ .

The decay of the  $Au+Au$  source (bottom panel of Fig.4 is also very well described by the statistical SMM model [24, 25]. A moderate contribution of radial flow (about 1  $A.MeV$ ) seems to be superimposed to the thermal excitation energy and the freeze-out density of this system, evaluated from the backtracing of experimental data as about 1/3-1/6 [25] of the normal density. The apparent exponent  $\tau_{eff}$  of the charge distribution is about 1.2 and

again the deviation from a power law behavior could be due in this case to the distance from the critical point [26] or to some other (size or entrance channel dependent) physical effects [27].

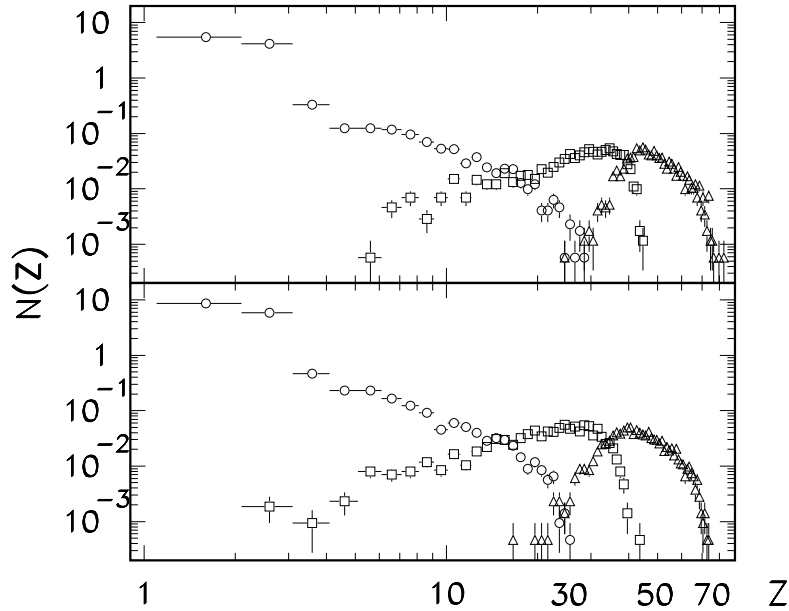


FIG. 5: Charge distribution of the largest fragment (triangles), the second largest (squares) and the remaining fragments (circles). Upper (lower) panel: central 25 (35) A.MeV Au+Cu events.

The same kind of agreement with statistical models is also observed, for all the considered reactions, for the charge partitions [24, 25] as well as for the fragment kinetic energies. The close similarity between statistical models and data, together with the isotropy of fragment emission (see Fig.3), suggests that this set of data can be analyzed an analysis in terms of thermal scaling.

To better understand the low value of  $\tau_{eff}$  for the  $Au + Cu$  central collisions, we show in Figure 5 the charge distribution of the biggest, second biggest and remaining fragments for both samples. One can see that the charge distribution of light fragments (circles) is steeper than the total distribution and that the flattening, resulting in  $\tau_{eff} \approx 1.4$ , is mainly caused by the second largest fragment, whose distribution covers a wide charge range.

In the next Section we give an interpretation of this behavior.

## B. Prompt or sequential emission?

As suggested in Ref. [28], the observed tail towards small  $Z$  values of the second largest fragment could be due to secondary decay of the largest primary fragment formed at the freeze-out, because of the reduced fission barriers of a source heavier than the  $QP$  one. According to this interpretation, fragments generated later than the freeze-out time should keep memory of their later emission by showing a strong velocity correlation. This should be apparent in the two-fragment velocity correlation function, defined as

$$1 + R(v_{red}) = C \frac{Y(v_{red})}{Y_{back}(v_{red})} \quad (5)$$

where  $v_{red} = (\vec{v}_i - \vec{v}_j) / \sqrt{(Z_i + Z_j)}$  is the reduced relative velocity of fragments  $i$  and  $j$  with charges  $Z_i$  and  $Z_j$ ;  $Y(v_{red})$  and  $Y_{back}(v_{red})$  are the coincidence and background yields for fragment pairs of reduced velocity  $v_{red}$  and  $C = N_{back}/N_{coinc}$  where  $N_{coinc}$  and  $N_{back}$  are the total number of coincidence and background pairs. The background yield was constructed by means of the mixed event technique [29].

This correlation function is in principle affected by a space-time ambiguity. However, if the density of the sources is comparable (as indicated by statistical model predictions) this observable measures the fragment formation time.

Figure 6 displays the correlation functions of the reduced velocity for all the sets of central events. These observables are also compared to the correlations obtained from  $QP$  events at the same excitation energy as the central sets.

For central  $Au + C$  events at 25 A.MeV the correlation function is very similar to the  $QP$  one, especially when only fission events are considered (dotted line). The peak at  $v_{red} \approx 10$  ( $c/1000$ ) corresponds to the Coulomb reduced velocity of two touching charged spheres.

For central  $Au + Cu$  events the correlation function of the reduced velocity between the two heaviest fragments in each event signals emission times longer than in the  $QP$  decay at the same excitation energy. The Coulomb hole is narrower than in the  $QP$  case and the peak corresponding to the reduced velocity of two touching charged spheres, observed in the  $Au + C$  reaction, is still present even if the excitation energy of the source is larger.

For the  $Au + Au$  central collisions the correlation function of the reduced velocity (Fig.6 bottom panel) of the two heaviest fragments does not give indications of a late emission.

Several interpretation of this behaviour can be given. One is that for  $Au + Au$  central

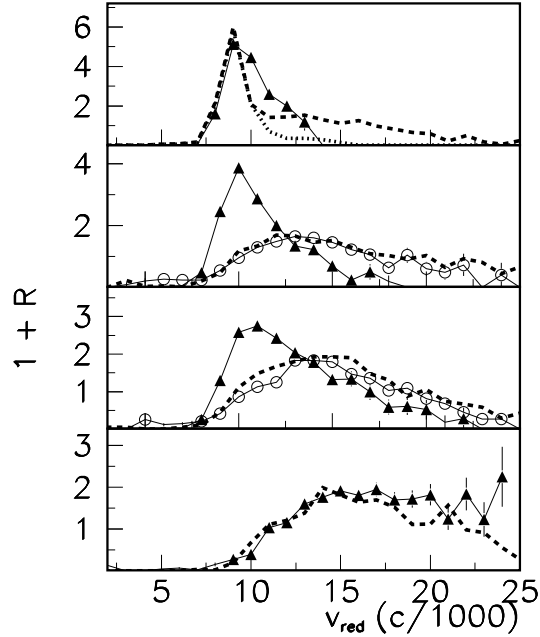


FIG. 6: Correlation functions of the reduced velocity for the two largest fragments in each event. From top to bottom: central  $Au + C$  events at 25 A.MeV,  $Au + Cu$  at 25, 35 A.MeV and  $Au + Au$  at 35 A.MeV. Triangles: correlation between detected fragments, open symbols: the same correlation after re-clusterization for central events(see text). Dashed lines: QP correlation at the same excitation energy as the corresponding central events.

events all the detected fragments were originated at the freeze-out time. Another alternative interpretation is that the increased Coulomb strength with respect to a  $Au$  source also affects the decay of fragments other than the largest one.

More sophisticated correlation techniques would be needed to answer this question.

For the  $Au + Cu$  reactions we can use the correlation function information to backtrace the sequential emission. We reclusterize the two heaviest fragments with a Gaussian shaped probability distribution, centered at the Coulomb reduced velocity and with a width given by the left tail of the correlation function. When the two heaviest fragments are reclusterized, they are replaced in the event by a primary fragment with a charge equal to the sum of their charges and a velocity vector given by the weighted mean of their velocities. As shown in Figure 6, after this procedure the correlation function has a very similar shape to the QP

one in the same excitation energy range.

### C. Critical exponents

After the backtracing of secondary fission the cluster size distribution for the central collisions  $Au + Cu$  at 25 and 35 A.MeV are in very good agreement with the QP size distributions at the same excitation energy (see Fig.7). In particular the 35 A.MeV reaction

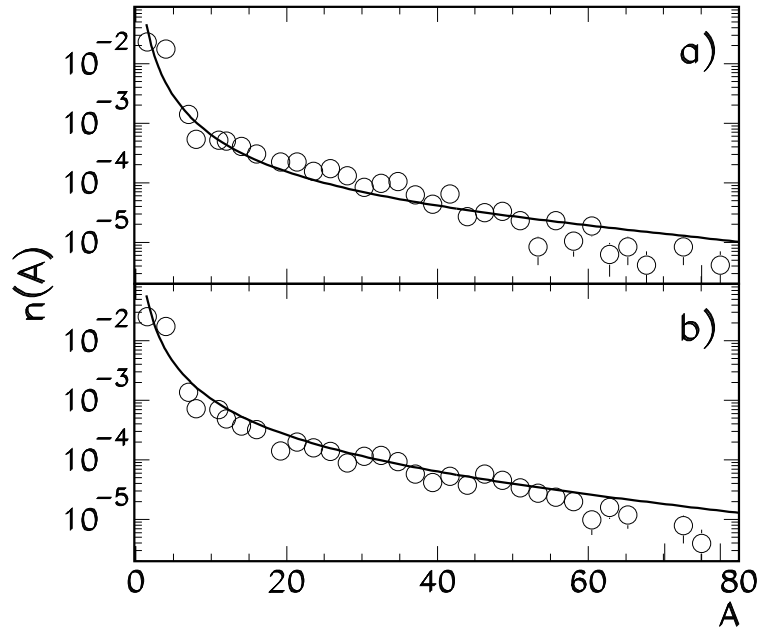


FIG. 7: Cluster size distribution for central  $Au + Cu$  events (open symbols), after re-clusterization of the two heaviest fragments with the procedure described in the text. The line represents the power-law from Eq.s(2,3,4) describing the QP events at the same excitation energy as central  $Au + Cu$  25 A.MeV collisions (top panel) and  $Au + Cu$  35 A.MeV collisions (bottom panel).

follows a power-law with  $\tau \approx 2$  as appears from the bottom panel of Fig.7. The fact that at similar excitation energies the central and peripheral sources show a similar fragment distribution strongly supports the thermal scaling.

In addition this means that, at least up to a source charge around 100, the increase of the Coulomb in the entrance channel only affects the decay of primary fragments, but not the bulk multifragmentation.

A power-law with exponent  $\tau \approx 2$  corresponds to partitions with very large size fluctuations [30], as signaled by the Campi plot of the central events (Fig.8), showing a “liquid” as well a “gas” branch.

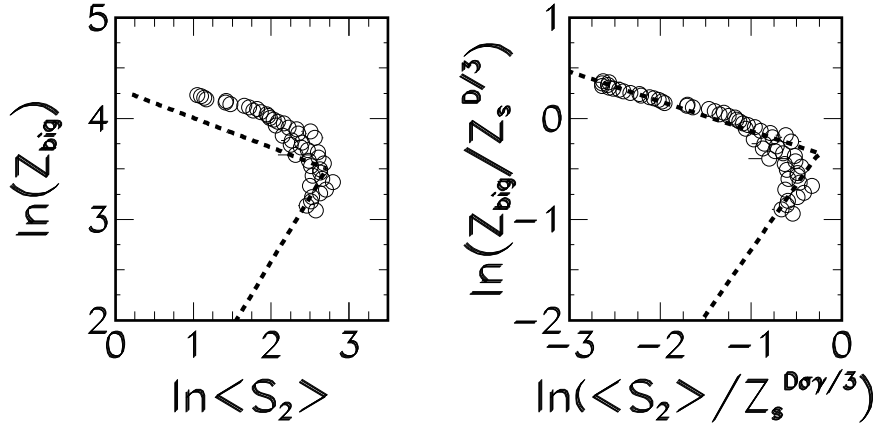


FIG. 8: Campi plot for the QP source (dashed line) and for Au + Cu 35 A.MeV central collisions (symbols). In the left panel the unscaled distribution is given, in the right panel scaled moments are shown.

It has to be noted, however, that a bimodal shape of the Campi plot is a necessary, but not sufficient, signal to claim the observation of a phase transition. Indeed simulations, which do not contain criticality, but only take into account the phase space [18] can produce Campi-plots apparently similar in shape. Only critical exponents [31] allow to identify criticality.

A strong check of compatibility among QP critical events and Au + Cu central events consists in the finite size scaling of the moments of the size distribution.

In Ref. [32] it has been shown that, as for percolation events, in finite nuclear systems near the critical excitation energy the size of the largest cluster and the second moment scale for the size of the system following the hyper-scaling relation [18, 32].

Following Ref. [32] the largest cluster size is expected to scale as  $S^{D/3}$ , where  $S$  is the size of the system,  $D = \frac{d}{\tau-1}$  is the fractal dimension,  $d = 3$  is the Euclidean dimension. The second moment  $S_2$  is expected to scale as  $S^{D\sigma/3}$ .

In the right panel of Fig.8 the correlation between the size of the largest fragment and the average second moment is shown for the central source, scaled [32] via the critical exponents of the QP source [3]. The observed agreement shows again the validity of the scaling [33] and the compatibility of critical exponents for the two systems.



In this section we have presented “compatibility” checks between the static observables of emitting sources, different in size and in the way they were formed. However, our aim is to extract a complete set of critical exponents also for sources formed in central collisions.

The procedure adopted for the QP in Ref. [3] cannot be applied to central collisions, since the excitation energy is distributed in a very narrow interval. However we have shown in Section III that even for sets of data that do not contain the critical point it is possible to get information on critical excitation energy and critical exponents by working with the Fisher scaling function eq.(2).

## V. FISHER SCALING FOR CENTRAL COLLISIONS

In order to get critical parameters for the central events, independently of the information extracted from the QP data, the fitting procedure described in Sect.III has been applied to the four sets of central events discussed above.

<b>Central collisions</b>	$\tau$	$\sigma$	$E_c^*$ (A.MeV)	$c_0$	$\chi^2$
Au+C 25 A.MeV	$2.0 \pm 0.6$	$0.64 \pm 0.02$	$4.5 \pm 0.1$	$10.0 \pm 0.2$	7.8
Au+Cu 25 A.MeV	$2.10 \pm 0.04$	$0.60 \pm 0.02$	$4.4 \pm 0.1$	$10.0 \pm 0.6$	1.8
Au+Cu 35 A.MeV	$2.05 \pm 0.04$	$0.68 \pm 0.03$	$4.5 \pm 0.2$	$9. \pm 1.$	1.3
Au+Au 35 A.MeV	$2.1 \pm 0.1$	$0.68 \pm 0.03$	$4.51 \pm 0.01$	$10.0 \pm 0.1$	1.7
All central	$2.05 \pm 0.02$	$0.66 \pm 0.02$	$4.40 \pm 0.03$	$13.0 \pm 0.4$	2.0

TABLE III: Values of the critical exponents  $\tau$ ,  $\sigma$ , critical excitation energy  $E_c^*$ , surface energy coefficient  $c_0$  and  $\chi^2$  of the Fisher scaling fit trough Eq.s(2,3,4).

The resulting scaling functions are shown in Figure 9 and the corresponding critical parameters are reported in Table III.

Also the data samples not covering the critical region point to the same critical energy and to compatible critical exponents. The fit is of high quality and the values of  $\Delta\mu$  at  $E_c^*$  are compatible with zero, within the error, except for the compound nucleus de-excitation events ( $Au + C$  reaction). In this case the value of  $\Delta\mu$  at  $E_c^*$  is large ( $2.9 \pm 0.06$  A.MeV) and the quality of the fit is poor. For this reaction, however, the excitation energy is very far from the critical one. As found for the QP events (see Section III) and in the study

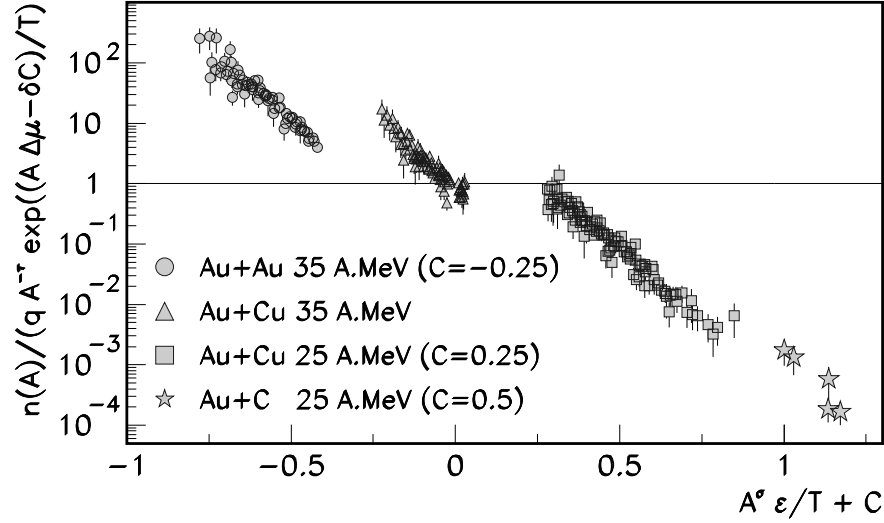


FIG. 9: *Fit of central events with the scaling function ansatz eq.(2). To visualize the results on the same picture a constant horizontal shift  $C$  is given to the distributions.*

performed on a Lattice Gas [21], an approximate description of the critical region can be provided by events containing only information on the vapor.

To check whether the scaling function (2) is able to describe the decay of finite charged nuclear matter, independently on the size of the source, a subset of events of equal statistics has been selected for the four sets of central events (1000 events for each reaction) and Fisher scaling (2) has been repeated on this sample. The resulting scaling function is displayed in Fig.10 and the parameters are again reported in Table III (label : 'All central'). The good quality of the scaling and the perfect agreement of the critical parameters with the Quasi-Projectile results are a striking proof of the universality of the scaling: the critical behavior and the whole shape of the scaling function are independent both on the size of the system and on the entrance channel. This implies that the Fisher scaling technique is extremely powerful and the determination of the critical parameters is robust with respect to the possible effects induced by the Coulomb interaction and by the reaction mechanism.

A word of caution is however necessary. In Section II we have presented a comparable quality scaling obtained with the RG ansatz (1) which applies to generic critical phenomena like percolation, not necessarily connected to a thermal transition. It is also well known that the liquid-gas critical exponents are very close to the percolation ones. Therefore other non static observables have to be analyzed before one can identify the transition as belonging to

the liquid-gas universality class, but this is beyond the aim of this paper [36].

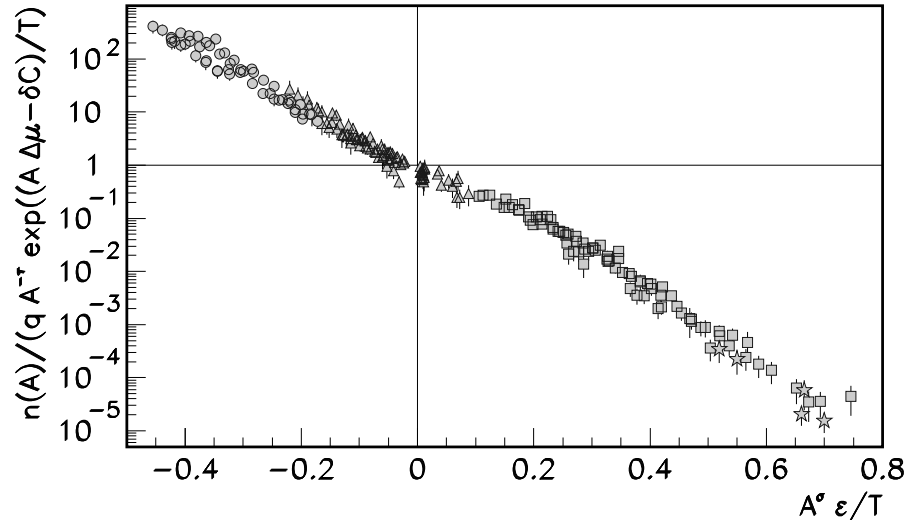


FIG. 10: *Simultaneous fit of an equal statistics subsample of the central events with the scaling function ansatz eq.(2). Symbols as in Fig.9.*

## VI. CONCLUSIONS

The decay of the Quasi-Projectile formed in peripheral 35 A.MeV  $Au + Au$  collisions has been compared to different sets of central events in terms of critical partitions and critical exponents.

All reactions are compatible with a critical behavior at an excitation energy of about 4.5 A.MeV, with critical exponents for the size distribution  $\tau \approx 2, \sigma \approx 0.65$ . Analyzing the velocity correlations between the two heaviest fragments we have demonstrated that fission is an important deexcitation channel for the secondary decay of heavily charged systems ( $Z_{source} \approx 100$ ). If this decay is back-traced we observe a perfect scaling with the size of the source between the peripheral QP events ( $Z_{source} \approx 80$ ) and the central  $Au + Cu$  ones ( $Z_{source} \approx 100$ ). On the other hand the size distribution of central  $Au + Au$  events is flatter than the QP one at a compatible deposited energy, and this fact cannot be ascribed to secondary fission.

The impressive quality of the scaling and the compatibility of the results of central and peripheral collisions does not demonstrate unambiguously the thermal nature of the transition, though it certainly is a strong circumstantial evidence for its existence. Indeed the

shape of the scaling function (i.e. the parameters  $c_0$  and  $\Delta\mu$ ) depends non negligibly on the technical assumptions made in the procedure of the fit and a similar scaling is obtained with the ansatz Eq.(1) that does not assume a thermal nature for the transition. This means that the different size distribution (implying a different behavior for  $\Delta\mu$ ) observed for the  $Au + Au$  system can be ascribed to a different thermodynamical path for the state variables explored in central collisions of symmetric systems, but also to non thermal effects due either to the entrance channel (signaled by the onset of collective flow [4]) or to the high charge of the system (Coulomb explosion for too heavily charged sources [2, 6]).

The scaling “per se” does not determine the order of the transition either. Indeed in many different statistical calculations [21, 26, 34, 35] first order phase transitions in finite systems lead to observations typical of continuous transitions including critical behaviors and critical exponents. Further work to assess this point is in progress [36].

The authors would like to acknowledge the *Multics-Miniball* collaboration, which has performed the experiments. The authors are also grateful to P. F. Mastinu and P. M. Milazzo for a critical reading of the manuscript.

This work has been partially supported by NATO grants CLG-976861 and by grants of the Italian Ministry of Instruction, University and Research (contract COFIN99).

- 
- [1] J. E. Finn *et al*, Phys. Rev. Lett. **49** (1982) 1321; X. Campi, Phys. Lett. **B208**, 351 (1988).
  - [2] M. L. Gilkes *et al.*, Phys. Rev. Lett. **73**, 1590 (1994), J.B.Elliott *et al.*, Phys.Lett. **B418** (1998) 34; R.P.Scharenberg *et al.*, Phys.Rev.**C64** (2001) 054602.
  - [3] M.D’Agostino *et al.*, Nucl.Phys. **A650** (1999) 329.
  - [4] W. Reisdorf *et al.*, Nucl.Phys. **A612** (1997) 493; W. Reisdorf, Progress of Theoretical Physics Supplement, No.**140** (2000) 111.
  - [5] A. Botvina *et al.* Nucl. Phys. **A584** (1995) 737.
  - [6] C. Williams *et al.* Phys.Rev. **C55** (1997) R2132, J. B. Elliott *et al.* Phys.Rev. **C59** (1999) 550, C. Williams *et al.* Phys.Rev. **C59** (1999) 550.
  - [7] M. D’Agostino *et al.*, Phys. Rev. Lett. **75** (1995) 4373.
  - [8] M.F.Rivet *et al.*, Phys.Lett. **B430** (1998) 217.
  - [9] P. Danielewicz, Phys. Rev. **C51** (1995) 716.

- [10] J.Pan and S. Das Gupta, Phys. Rev. **C53** (1995) 1319; S. Pratt *et al.* Phys. Lett. **B349** (1995) 261.
- [11] M.E.Fisher, Physics vol. 3 (1967) 255.
- [12] J.B.Elliott *et al.*, Phys.Rev.Lett.88 (2002) 042701 and arXiv:nucl-ex/0104013.
- [13] M.D'Agostino *et al.*, Phys.Lett. **B368** (1996) 259.
- [14] M.D'Agostino *et al.*, Phys.Lett. **B473** (2000) 219, Nucl. Phys.**A699** (2002) 795.
- [15] P. M. Milazzo *et al.*, Phys. Rev. **C58** (1998) 953.
- [16] J. P. Bondorf, A. S. Botvina, A. S. Iljinov, I. N. Mishustin, K. Sneppen, Phys. Rep. **257** (1995) 133.
- [17] D. Stauffer and A. Aharony, Introduction to percolation theory (Taylor and Francis, London 1992).
- [18] J. B. Elliott *et al.*, Phys. Rev. C **62**, 064603 (2000).
- [19] J.A.Lopez and C.O.Dorso, 'Phase transformations in nuclear matter', World Scientific (2000).
- [20] J.B.Natowitz *et al.*, Phys. Rev. **C 65** (2002) 34618.
- [21] F.Gulminelli *et al.*, nucl-th/0201046 and Phys. Rev.**C** (2002) 51601.
- [22] J. F. Lecomte *et al.*, Nucl. Instr. and Methods A441 (2000) 517.
- [23] R. J. Charity *et al.*, Nucl. Phys. A483 (1988) 371.
- [24] M.D'Agostino *et al.*, Phys.Lett. **B371** (1996) 175.
- [25] P. Desesquelles *et al.*, Nucl. Phys. **A633** (1998) 547.
- [26] A.H.Raduta *et al.*, Phys. Rev. C **65**, 034606 (2002).
- [27] P. M. Milazzo *et al.*, submitted to Phys. Rev. **C**.
- [28] A.J.Cole, Phys. Rev. **C65** (2002) 031601.
- [29] R. Trockel *et al.*, Phys. Rev. Lett. **59** (1987) 2844.
- [30] C.O. Dorso and J.A. Lopez, Phys. Rev. **C 64** (2001) 027602.
- [31] A. Bonasera, M. Bruno, C. Dorso and P. F. Mastinu, "Critical phenomena in nuclear fragmentation", La Rivista del Nuovo Cimento vol.23, n.2 (2000).
- [32] H. R. Jaqaman and D. H. E. Gross, Nucl. Phys. **A524** (1991) 321.
- [33] L.G.Moretto *et al.*, Nucl.Phys. A681 (2001) 239.
- [34] F.Gulminelli, Ph.Chomaz, Phys.Rev.Lett.82 (1999) 1402.
- [35] J.M.Carmona *et al.*, Phys.Lett. B, in press.
- [36] M.D'Agostino *et al.*, in preparation.